16th World Conference on Earthquake Engineering, 16WCEE 2017

Santiago Chile, January 9th to 13th 2017

Paper N° 3678

Registration Code: S-D1464727187

MULTIPHYSICS MODELING, EXPERIMENTAL VALIDATION AND BUILDING IMPLEMENTATION OF VISCOUS FLUID DAMPERS

C. Frings[1], R. Zemp[2], J.C. De La Llera[3]

[1] *Sub Technical Manager, Nüyün_Tek S.p.A., cfrings@nuyuntek.cl*
[2] *Technical Manager, Nüyün_Tek S.p.A., rzemp@nuyuntek.cl*
[3] *National Research Center for Integrated Natural Disaster Management, CONICYT/FONDAP/15110017, Pontificia Universidad Católica de Chile, jcllera@ing.puc.cl*

Abstract

The scope of this article is the design, testing, implementation and health-monitoring of viscous fluid dampers in a real building. First, a numerical model that captures the complex fluid dynamics and thermal behavior of the flow inside the damper is presented. Since these two phenomena are coupled, a multiphysics model was developed. The model was able to predict the force-velocity relationship, the pressure increase due to thermal expansion of the fluid, and the force decline as the fluid viscosity decreases, which are key aspects for satisfactory and efficient damper design. Using this model, the design of 78 units for a two tower 19-story building complex was accomplished. The devices, with a nominal capacity of 1275 *kN*, were developed in Chile and one unit, identical to the others, was shipped to the ATLSS Engineering Research Center at Lehigh University to undergo extensive testing in order to ensure the damper´s adequate performance and, at the same time, validate the numerical models used. Included among the many tests were: (*i*) harmonic cycles at maximum design velocity (362 *mm*/*s*); (*ii*) seismic input; and (*iii*) life cycle tests. In particular, the seismic movement displacement signal was obtained from a response-history analysis of a FE building model, subjected to an earthquake acceleration record compatible with the Peruvian seismic code. The displacement history of the most demanded device was used as input for the dynamic actuator at the Lab. Experimental results turned out to be in excellent agreement with numerical results in terms of output force, pressure increase, and viscosity decrease. Furthermore, damper performance was optimal, satisfying the energy dissipation demand and producing a force output with small deviation from nominal values. Finally, two of the 78 devices installed in the building were connected to a health-monitoring system including displacement sensors, accelerometers, internal pressure transducers, and temperature sensors. These were wired to a data acquisition system which can be monitored remotely online. The objective is to record damper displacement and output force during a future seismic event, which will provide valuable information on the real damper and building performance.

Keywords: passive energy dissipation; viscous fluid damper; multiphysics; fluid dynamics; health monitoring

1. Introduction

Structural damage is inherent to buildings designed to undergo severe ground motions. Supplemental energy dissipation devices mitigate such damage by absorbing part of the mechanical vibration energy, thus decreasing the ductility demand on the primary structural elements. In particular, viscous fluid dampers are increasingly used for this purpose, because they present advantages such as: *i*) large amounts of dissipated energy relative to their size [13]; *ii*) ease of implementation in new or retrofit designs; *iii*) no need for replacement after earthquakes; and *iv*) an output force dependent on velocity, which tends to be out of phase with displacements, thus reducing structural response without increasing base shear and elastic forces [10].

The basic operating principle of these devices is the motion of a piston through a viscous fluid enclosed in a cylindrical housing. This movement forces fluid to pass from one chamber of the damper to the other through different types of orifices, being generally acknowledged that the type and shape of these orifices is a key aspect to control the behavior of the damper (e.g., [2], [4], [13], [14]). A schematic view showing the internal parts of a fluid viscous damper is presented in Fig. 1. Pressure relief valves and accumulators may be also included to limit internal pressure increase within the cylindrical housing.

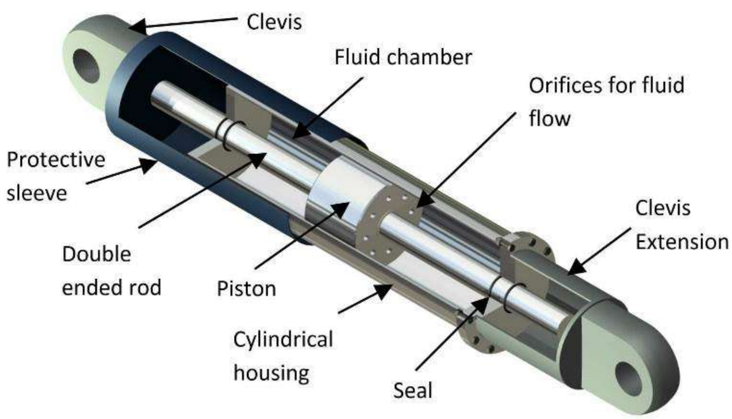

Fig. 1 – Internal parts of a viscous fluid damper.

It is commonly accepted that the output force of the damper is related to the velocity of its end supports by a power law. Thus, the force-velocity constitutive relationship is usually expressed as ([10], [13], [14]):

$$F = C \cdot |V|^{\alpha} \cdot \operatorname{sgn}(V) \tag{1}$$

where V represents the velocity input of the damper; C is a viscous coefficient; and the exponent α, the one that controls the behavior of the damper. In general, intermediate values of exponent α say, $0.2 < \alpha < 1.0$, are preferred for structural applications due to the adequate force control they produce [10]. Dampers with high α ($\alpha > 1.0$) may develop large forces that can damage braces and connections if unexpected high velocities occur during the structural motion; for instance, under near fault ground motion conditions [14].

This paper introduces first a numerical model of the fluid dynamics and heat transfer inside the damper, which are coupled phenomena. Then, the calculation of key results involved in damper design, such as the force-velocity relationship, pressure build-up due to thermal expansion of the fluid as energy is dissipated, and force decrease as fluid viscosity decreases with rising temperature, is explained. The multiphysics model developed was used in the design of 78 identical viscous dampers which were manufactured in Chile. One randomly selected unit was sent to ATLSS Engineering Research Center at Lehigh University to undergo extensive cyclic and earthquake testing. Therefore, a comparison of the experimental and numerical results is presented herein. Finally, the installation of the devices in a two tower, 19-story building is addressed, with emphasis on two units that were connected to a DAQ system to record displacement, acceleration, internal pressure, and temperature during a seismic event.

2. Multiphysics modeling

The main objective of the model is to solve the problem shown in Fig. 2: a piston surrounded by a viscous fluid in a closed housing is subjected to an arbitrary known displacement, representing any kind of movement (harmonic, seismic, etc.) imposed to the damper by an external source. This will create a pressure differential between the anterior and posterior chambers, forcing the fluid to move from one chamber to the other through passages. Because of the resistance to the flow, the piston will be subjected to stresses applied on its surfaces that will result in the damper's output force [5]. Solving for the generated velocity and pressure fields will allow to integrate these stresses and obtain the force-velocity constitutive relationship for the damper.

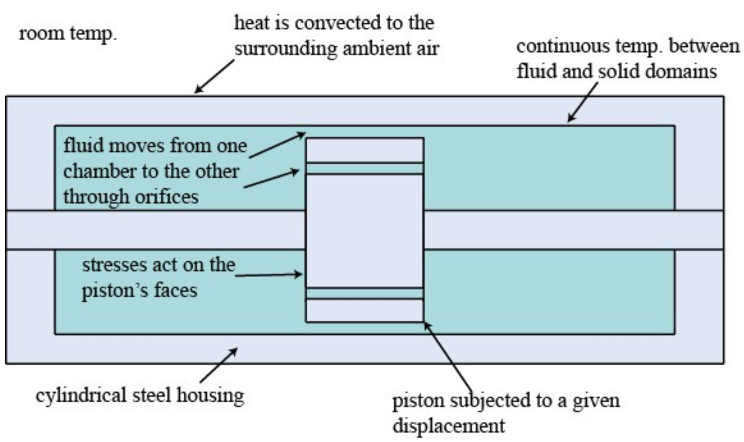

Fig. 2 – Schematic representation of the problem to solve.

Additionally, as the fluid flows back and forth it will heat up due to the work done and its viscosity, which is a measure of the intermolecular resistance of fluid layers in trying to slide past one another [7]. It is by this mechanism that kinetic energy is transformed into thermal energy. The fluid will conduct heat to the metallic parts of the casing and, in turn, the metallic casing will transfer heat into the surrounding environment. Hence, a further objective of this study is to determine the temperature field, in both, the fluid and the metallic components, i.e. the cylinder, piston, and rod.

As it will be shown, viscosity may be modeled to depend on the fluid temperature. Since fluid flow depends on viscosity, fluid dynamics and heat transfer equations are coupled by this variable. In the next sections, the governing equations will be presented briefly, but the detailed derivation of these equations and their limitations may be found elsewhere [9].

2.1 Fluid dynamics

The equations used to model flow inside the damper derive from basic continuum conservation principles. For incompressible flow (i.e. constant fluid density), conservation of mass leads to:

$$\nabla \cdot \mathbf{u} = 0 \tag{2}$$

where $\mathbf{u} = (u,v,w,t)$ is the velocity field. Fluid may be modeled compressible with a barotropic formulation [5], but it is computationally time consuming and not relevant for the results presented in this paper. Considering an isotropic fluid and using Stokes' assumption, conservation of linear momentum leads to:

$$\rho \frac{\partial \mathbf{u}}{\partial t} + \rho \mathbf{u} \cdot \nabla \mathbf{u} = -\nabla p + \nabla \cdot \mu \left[\nabla \mathbf{u} + \left(\nabla \mathbf{u} \right)^T \right] \tag{3}$$

where ρ is fluid density; $\nabla \mathbf{u}$ is a velocity gradient tensor; p is the pressure field; and μ is the dynamic viscosity of the fluid. The dynamic viscosity may be a constant, as in the case of a Newtonian fluid, or may be a function of the velocity field and fluid temperature, as it will be explained in section 2.3. Equations (2) and (3) are the Navier-Stokes equations for incompressible flow.

2.2 Heat transfer

Conservation of energy leads to the following equation, valid for fluids or solids:

$$\rho C_p \left(\frac{\partial T}{\partial t} + \left(\mathbf{u} \cdot \nabla \right) T \right) = \nabla \cdot \left(k \nabla T \right) + \tau : \mathbf{S} \tag{4}$$

where T is the temperature field; C_p is the specific heat of the medium; and k its thermal conductivity. The term $\mathbf{S}$ is the symmetric strain rate tensor, defined as:

$$\mathbf{S} = \frac{1}{2} \left[\nabla \mathbf{u} + \left(\nabla \mathbf{u} \right)^T \right] = \dot{\gamma} \tag{5}$$

and τ is the deviatoric or viscous stress tensor related to $\mathbf{S}$ by $\tau = 2\mu\mathbf{S}$. The term $\tau : \mathbf{S}$ represents the rate of work for changing the shape of a fluid element at constant volume and is known as the dissipation function. It acts as a source of thermal energy in the damper; more details can be found in [15]. Naturally, in solid domains $\mathbf{u}$ and $\mathbf{S}$ are zero, and heat is transferred only by conduction. Heat transfer between the cylinder and surrounding environment was modeled with a convection boundary condition.

2.3 Fluid properties

Generally, silicone oil, an organic silicon-based polymer, is used as a viscous damper fluid. It is a non-Newtonian fluid since it exhibits shear thinning, i.e., its viscosity decreases with increasing shear rate. This phenomenon is explained by the stretching of entangled molecules, permitting them to move in a more aligned manner, and hence, with less resistance [8].

If temperature is considered constant, the viscosity-shear rate constitutive relationship for silicone fluid may be modeled by the Yasuda-Carreau equation ([3], [6]):

$$\frac{\mu - \mu_\infty}{\mu_0 - \mu_\infty} = \left[1 + \left(\kappa \cdot \dot{\gamma} \right)^a \right]^{\frac{n-1}{a}} \tag{6}$$

where μ_0 is the zero shear-rate viscosity; μ_∞ is the infinite shear-rate viscosity (zero in this case); κ is a characteristic time (the reciprocal of the intercept between the power law line and the zero shear rate viscosity); n is the power law region exponent; a represents the width of the transition region between Newtonian and power law behavior; and $\dot{\gamma}$ is the shear rate magnitude defined in equation (5).

Although less pronounced than in most liquids, silicone oil exhibits a decrease in viscosity with rising temperature. This can be incorporated into equation (6) by multiplying μ_0 and κ by a temperature dependent shift factor $Z(T) = \exp(b/T - b/T_{ref})$, where b is a parameter and T_{ref} is a reference temperature corresponding to μ_0 and κ [12]. Hence, the shear and temperature effects can be modeled by:

$$\mu\left(\mathbf{u},T\right)=Z\left(T\right)\cdot\mu_0(T_{ref})\left\{1+\left[Z\left(T\right)\cdot\kappa(T_{ref})\cdot\dot{\gamma}\right]^a\right\}^{\frac{n-1}{a}} \tag{7}$$

Please note that as temperature increases, the value of μ decreases. A lower viscosity means there is less resistance to move the fluid from one chamber to the other, resulting in a smaller output force for the same piston velocity. By incorporating equation (7) into the model, this effect shows up in the force-velocity analysis.

Equations (2) through (7) form a system of five equations and five unknowns, all coupled by Equation (7). They are derived from an Eulerian standpoint, in which domain mesh nodes remain fixed, the usual practice in computational fluid dynamics. Nevertheless, in this particular problem, the fluid domain continually changes its shape as the piston strokes. Therefore, these equations were solved with the commercial software CFD-Flo, a finite volume based computational fluid dynamics program included in ANSYS [1], using deformable grids. Boundary displacements were prescribed (the piston displacement in this case), to which the domain conforms by solving a displacement diffusion equation at the beginning of each time step, preserving the relative distribution of the initial mesh [1]. Fig. 3 shows an axis-symmetrical domain in which the grid conforms to the movement of the piston at different time steps.

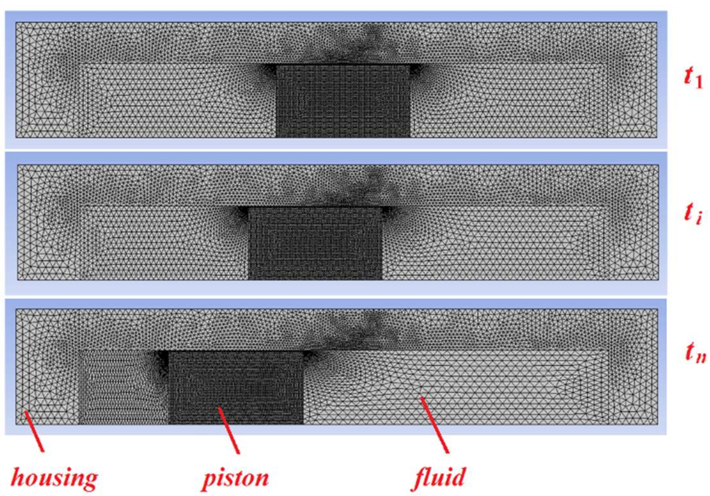

Fig. 3 – Mesh deformation at different time steps.

2.4 Model post-processing

Once the velocity, pressure, and temperature fields are solved, the quantities of interest may be determined. To obtain the damper's output force, we first note that the right term in equation (3) represents the surface stresses acting on a fluid element. Integrating these terms along the piston boundary results in the damper's force. Performing this calculation at all solution time steps yields the force-velocity constitutive relationship for the device. The increase in internal pressure due to fluid thermal expansion can be calculated using equation (8):

$$\Delta p=\zeta\cdot\Delta T \tag{8}$$

where $\Delta p = p - p_0$ is the pressure increase in relation to the initial pressure p_0; ζ (*bar/K*) is the thermal-pressure coefficient which can be readily obtained from fluid data sheets or handbooks; and $\Delta T = T - T_0$ is the temperature increase in relation to the initial fluid temperature T_0. Consequently, the expression $\zeta \cdot \Delta T$ is averaged over the entire fluid domain at each time step to obtain the corresponding pressure increment.

3. Manufacturing

The previous model was used in the design of 78 identical viscous dampers to be installed in an office building as described later. The model was used specifically for the detailed design of the piston geometry to satisfy the required nominal properties for the dampers. In relation to Equation (1), these were C = 1745 $kN{\cdot}(s/m)^{\alpha}$ and α = 0.3. Additionally, the model was used to estimate the demand on the main cylinder acting as a pressure vessel. The devices were designed for a maximum force of 1275 *kN*, a stroke of +/- 50 *mm*, and an energy dissipation capacity of 1600 *kJ*. A sketch of the device connected in a diagonal configuration (as in the building) and a finished unit may be seen in Fig. 4.

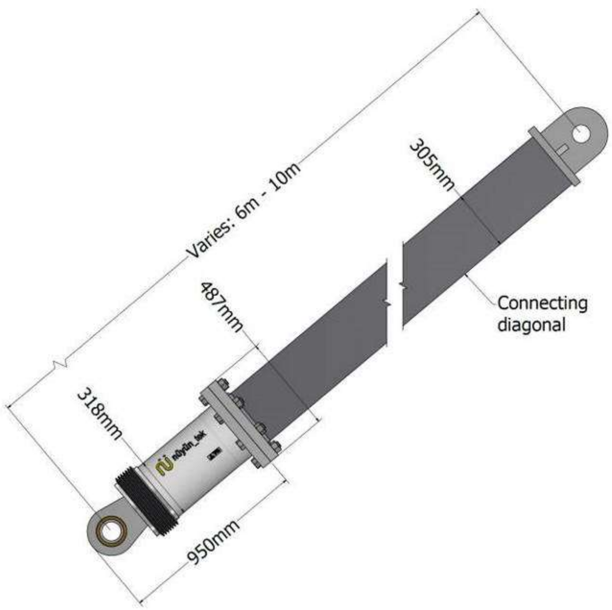

Fig. 4 – General dimensions of the damper and the diagonal brace that connects it to the building and a finished unit installed in a test rig.

4. Experimental Testing

The experimental setting for the tests is shown in Fig. 5. The viscous damper was connected in series to a dynamic actuator that imposes a prescribed displacement along its longitudinal axis. Damper displacement was measured with an LVDT between the clevis and main cylinder, output force was measured with a load cell connected between the damper and the actuator, and two pressure sensors were connected to the damper, one at each chamber.

The following tests were carried out: three cycles at maximum design velocity (Test 1), seismic movement (Test 2), and a life cycle test (Test 3). Test 1 consisted on sinusoidal displacement with A = 48 *mm* (the maximum design displacement) and f = 1.2 *Hz*, to generate the maximum design velocity of the device, 362 *mm/s*. For Test 2, a seismic displacement signal was obtained from the time-history analysis of the finite element model of the building in which the dampers were installed. A compatible record with the Peruvian seismic design code [11] was created using a seed record from the 1985 Chile earthquake. The displacement history of the most demanded device in terms of energy dissipation was used as input for the dynamic actuator in the Lab. Finally, Test 3 consisted on 60 cycles at A = 48 *mm* and f = 0.05 *Hz*.

A comparison of the experimental and theoretical force-velocity and force-displacement curves for Test 1 is presented in Fig. 6. The model is very accurate in capturing the non-linear behavior of the damper. The measured max force (absolute value) was 1258 *kN*, while the peak model force was 1272 *kN*, showing a 1.1% difference with the estimated value. According to the nominal properties (C = 1745 $kN{\cdot}(s/m)^{\alpha}$ and α = 0.3) and Equation (1), damper force for the maximum measured velocity, i.e. 364.8 *mm/s*, should be 1289.5 *kN*. This value is just 2.4% different from the actual measured maximum force, showing that the piston geometry was successfully designed to satisfy the required nominal values. Note that the experimental results show hysteresis in the force-velocity relationship while numerical results do not. This is a consequence of the fluid model, which assumes incompressibility. As mentioned, compressibility may be incorporated, but it is computationally time consuming and does not have a significant impact on the required results, such as maximum force or the amount of dissipated energy.

Fig. 5 – Damper connected to the test rig at ATLSS Engineering Research Center at Lehigh University in Bethlehem, USA.

Furthermore, the model is also successful in accurately representing the decrease in maximum cycle force for successive cycles, as it can be clearly observed in Fig. 6. It is to be noted that Test 1 was extremely demanding on the damper in terms of power with 600 *kJ* of energy dissipated in 2.5 *s*, i.e. 38% of the total design energy capacity, which is to be dissipated during a 75 *s* long earthquake. This explains the accelerated force reduction between cycles.

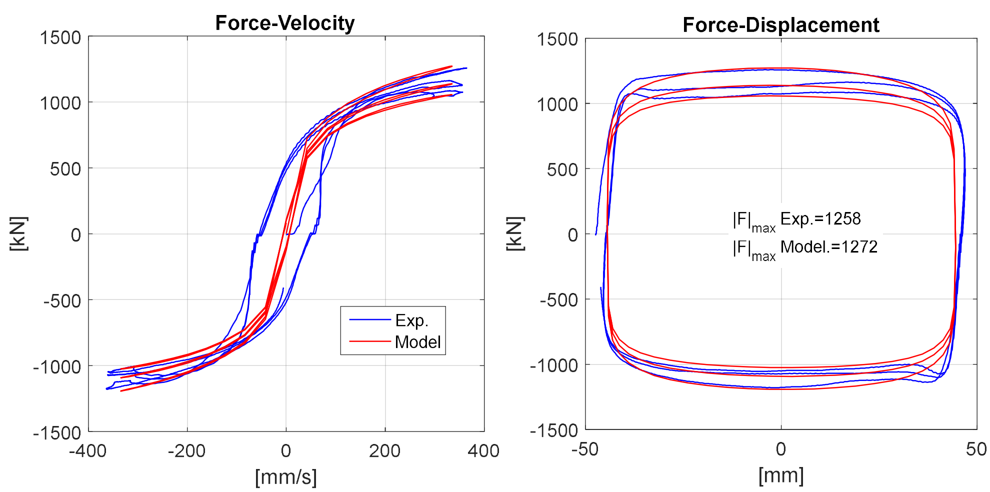

Fig. 6 – Comparison of experimental and model results for Test 1.

Shown in Fig. 7 is the seismic displacement signal corresponding to Test 2. A comparison between the experimental force-velocity and force-displacement curves with the model results for Test 2 is presented in Fig. 8. Results show again very good agreement. Furthermore, Fig. 9 shows the accumulated dissipated energy for the test. During the 75 *s* seismic displacement, 1654 *kJ* were dissipated by the damper without any damage or leaking.

Likewise, Fig. 9 shows that the model is quite accurate in predicting the internal pressure increase due to energy dissipation within the damper. The experimental pressure increase was obtained by averaging both pressure transducers at each time step and by subtracting the initial pressure value of the test.

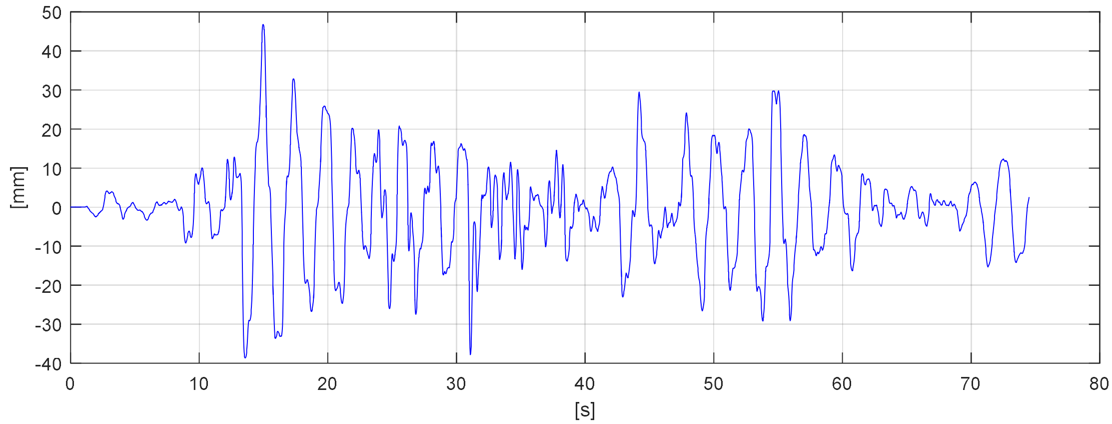

Fig. 7 – Seismic displacement input for the actuator for Test 2.

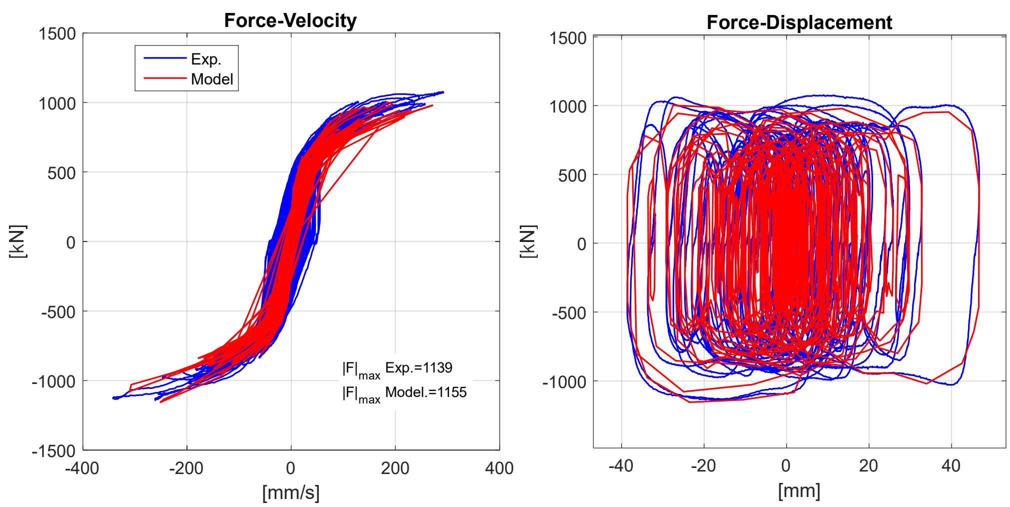

Fig. 8 – Comparison of experimental and model results for Test 2.

A comparison of the experimental and numerically predicted increase in internal pressure due to fluid heating at the end of each of the three tests is presented in Table 1. The experimental pressure increase was obtained by averaging both pressure transducers immediately after the end of the test and subtracting the initial pressure value. The multiphysics model was again very accurate in predicting these values. Calculating Δp is key to damper design, since the cylinder housing, the main part of the device, acts as a pressure vessel and needs to be designed for a maximum plausible pressure. The use of such a model significantly hastens the prototyping process. At best, pressure increase may only be roughly estimated using analytical methods, and hence, the usefulness of the model proposed. An important advantage of this model is that any arbitrary displacement may be assigned to the piston, allowing to numerically estimate the pressure increase using an actual design earthquake displacement signal. This allows for tailor-made designs for a given structure and viscous damping system.

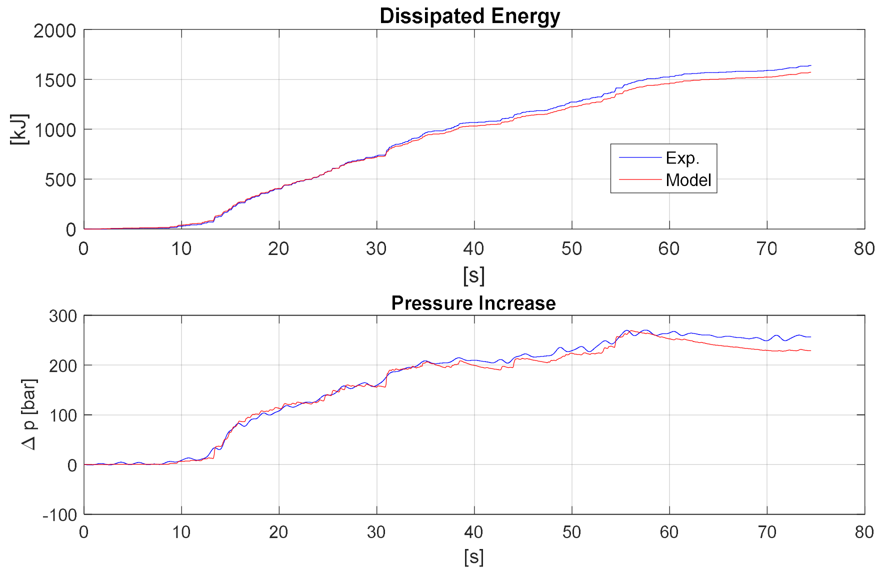

Fig. 9 – Top: comparison of the experimental and model accumulated dissipated energy during Test 2; bottom: comparison of the measured and modeled pressure increase due to thermal expansion of the fluid inside the damper during Test 2.

Table 1 – Measured and modeled pressure increase due to fluid heating for each test.

Test	**Experimental** Δp *(bar)*	**Model** Δp *(bar)*
1	246.1	269.6
2	253.2	229.0
3	460.7	445.8

5. Implementation

The 78 manufactured viscous damper units were installed in *Panorama Plaza de Negocios*, a two tower reinforced concrete building complex in Lima, Peru. The goal of the design was to improve the seismic performance of the structure. Each tower has 19 stories and 8 underground levels, and the lateral resisting system of the structure combines moment resisting frames and shear walls. Thirty nine viscous dampers were installed in each tower in metallic diagonal braces connecting every other floor. A general view of the building and how the devices are distributed and connected to the structure is shown in Fig. 10.

Two of the 78 devices were instrumented and connected to a DAQ to be remotely monitored online. Each damper has redundant displacement sensors (a laser sensor and a string pot), two pressure transducers (one at each chamber), a temperature sensor in contact with the fluid, and an accelerometer. The pressure transducers act as a load cell, since they enable to calculate the output force of the damper by multiplying the pressure difference between the two chambers by the piston area.

The DAQ is programmed to activate the sensors and make a reading every ten minutes in normal operation; however, if any of the accelerometers or displacement sensors exceeds certain threshold, the DAQ is triggered to record data at a sampling rate of 100 *Hz*. The objective is to acquire valuable information on the damper behavior during a severe seismic event, such as output force, displacement, velocity, dissipated energy, pressure increase, and fluid temperature increase. The system is connected to a UPS with a 12 hour autonomy to avoid a system shutdown when electrical power is cut off, as it usually happens during a severe seismic event. The deployment of the instrumented dampers at the fifth floor is indicated with star symbols in Fig. 10. One of the monitored dampers is shown in Fig. 11.

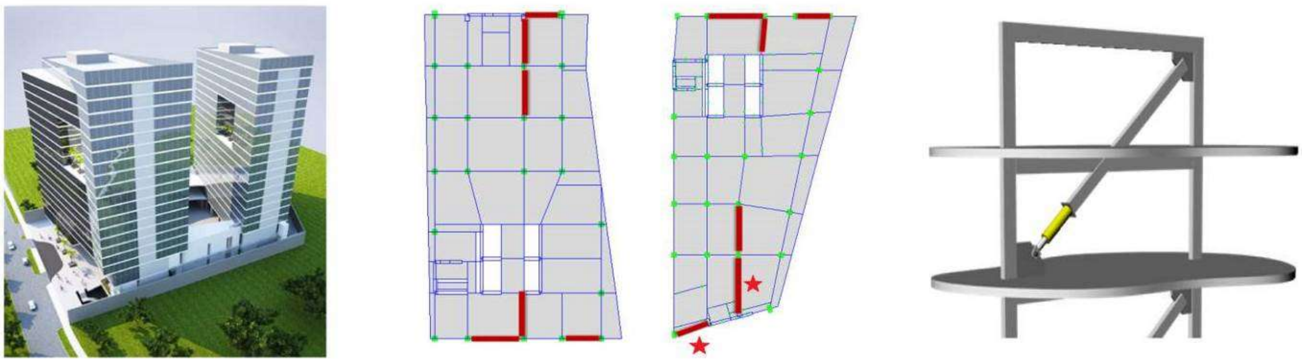

Fig. 10 – The left image shows a general view of the two towers, the middle image shows a plan view indicating the position of diagonals with viscous dampers, and the right image shows the configuration connecting every other floor. Red stars indicate the position of the monitored devices in the 5th floor.

Fig. 11: Instrumented damper in the building.

6. Conclusions

From this work it may be concluded that the multiphysics model presented herein proved to be a remarkably accurate and powerful tool for the design of viscous dampers. Important blind estimations for the force-velocity relationship, pressure increase in the main cylinder due to thermal expansion of the fluid, and force decrease as an effect of a decrease in viscosity, were successfully verified experimentally with a randomly selected damper unit tested in an independent laboratory in the US. Comparison between the numerically predicted force-velocity, force-displacement, temperature, and internal pressure results relative to the measured values leads to errors less than 9.6%. The model was used in the design of 78 viscous devices, which were manufactured in Chile and installed in a two-tower 19-story building in Peru. In order to gain relevant seismic information, two of these dampers were instrumented, and they are expected to provide useful feedback on the performance of these devices during a severe future earthquake.

7. Acknowledgements

This research has been sponsored by CORFO through project 13IDL4-25675, by the National Research Center for Integrated Natural Disaster Management (CIGIDEN) CONICYT/FONDAP 15110017, and by FONDECYT Grant 1141187. The authors are grateful for this support. Special thanks to the company GyM and Mr. Hugo Pineda and Jorge Castillo for their support during the installation of the viscous dampers, to Hector Sarmiento from Grupo Lander, to Proyecta for allowing the installation of the instrumented dampers in their offices, and to the structural engineers of the building and energy dissipation devices, Prisma Ingenieros and Sirve S.A.

8. References

[1] Ansys Inc. (2011): *ANSYS release 14.0*. Canonsburg, PA, United States.

[2] Cameron B, Makris N (2007): Viscous heating of fluid dampers under small and large amplitude motions: experimental studies and parametric modeling. *Journal of Engineering Mechanics,* 133(5), 566-577.

[3] Clasen C, Kavehpour P, McKinley G, (2010): Bridging tribology and Microrheology of thin films, *Applied Rheology*, 20(4), 45049-(1-13).

[4] Constantinou MC, Symans MD (1992): Experimental and analytical investigation of seismic response of structures with supplemental fluid viscous dampers. *National Center for Earthquake Engineering Research Rep. No. NCEER-92-0032*, State Univ. of New York at Buffalo, Buffalo, NY.

[5] Frings C, De La Llera JC (2011): Multiphysics modeling and experimental behavior of viscous dampers. *The 8th International Conference on Structural Dynamics, (EURODYN 2011)*, Leuven, Belgium.

[6] Ghannam M, Esmail N (1998): Rheological Properties of Poly(dimethylsiloxane). *Ind. Eng. Chem. Res.,* 37, 1335-1340.

[7] Hou CY (2008): Fluid dynamics and behavior of nonlinear viscous fluid dampers. *Journal of Structural Engineering*, 134(1), 56-63.

[8] Hou CY, Hsu DS, Lee YF, Chen HY, Lee JD (2007): Shear thinning effects in annular orifice viscous fluid dampers. *Journal of the Chinese Institute of Engineers*, 30(2), 275-287.

[9] Kundu KP, Cohen IM (2012): *Fluid Mechanics*. Elsevier Academic Press, 5th edition.

[10] Lee D, Taylor DP (2008): Viscous damper development and future trends. *The Structural Design of Tall Buildings*, 10, 311-320.

[11] Ministerio de Vivienda, Construcción y Saneamiento (2014): *Norma Técnica E.030: Diseño Sismorresistente Aprobada por Decreto Supremo N° 011-2006-Vivienda, Modificada con Decreto Supremo N°002-2014-Vivienda*. Lima, Perú.

[12] Swallow FE (2002): Viscosity of Polydimethylsiloxane Gum: Shear and Temperature Dependence from Dynamic and Capillary Rheometry. *Journal of Applied Polymer Science,* Vol. 84, 2533-2540.

[13] Symans MD, Constantinou MC (1998): Passive fluid viscous damping systems for seismic energy dissipation. *ISET Journal of Earthquake Technology*, 35(4), 185-206.

[14] Valdebenito G, Aparicio A, Alvarez J, López-Almansa F (2010): Passive Seismic Energy Dissipation Applying Fluid Viscous Damping Technology: A State of the Art Review. *Congreso Chileno de Sismología e Ingeniería Antisísmica*. Santiago, Chile.

[15] Winter HH (1987): Viscous dissipation term in energy equations. *Modular Instruction Series Volume 7: Calculation and Measurement Techniques for Momentum, Energy and Mass transfer*. American Institute of Chemical Engineers, C7.4, 27-35.